Mineralogical study of bassetite in relation to its oxidation

RENAUD VOCHTEN

Laboratorium voor chemische en fysische Mineralogie
Universiteit Antwerpen
Middelheimlaan 1, B-2020 Antwerpen, Belgium

EDDY DE GRAVE

Laboratorium voor Magnetisme
Rijksuniversiteit Gent
Proeftuinstraat 42, B-9000 Gent, Belgium

AND JOZEF PELSMAEKERS

Studiecentrum voor Kernenergie
Boeretang 200, B-2400 Mol, Belgium

Abstract

Bassetite and its fully oxidized phase have been synthesized and investigated, using powder diffraction, Mössbauer- and infrared spectroscopy, zeta-potential measurements and thermal analysis. Chemical analyses of the synthetic specimens prove that the general crystal-chemical formula corresponds to $Fe^{2+}_{1-x}Fe^{3+}_x[UO_2|PO_4]_2(OH)_x \cdot (7-x)H_2O$ where $0 \le x \le 1$.

For synthetic bassetite the space group is determined as $P2_1/m$ (C^2_{2h}) with cell parameters: $a = 6.98(4)$, $b = 17.07(4)$, $c = 7.01(7)$Å, $\beta = 90°32' \pm 5'$, $V = 835.2$Å^3, Z = 2 and the measured density 3.63 g/cm^3. Five of the strongest lines in the X-ray powder pattern are (as *d, I,hkl*) 8.616(100)(020); 2.2162(96)($\bar{3}$01); 3.4818(76)($\bar{2}$00); 4.9691(70)($\bar{1}$01); 2.9479(50) ($\bar{1}$22,$\bar{2}$21).

Fully oxidized synthetic bassetite with unknown space group belongs to the monoclinic system with cell parameters: $a = 6.958(5)$, $b = 6.943(5)$, $c = 21.052(5)$Å, $\beta = 90°92' \pm 5'$, $V = 1016.9$Å^3, Z = 2 and the measured density 3.00 g/cm^3. Five of the strongest lines in the X-ray powder pattern are (as *d,I,hkl*) 3.4843(100) ($\bar{2}$00,020), 4.9422(90)(013), 10.359(85)(002), 2.2010(77)(109,310,033,130), 3.3133(57)($\bar{2}$02).

The oxidation degree up to 40% can be determined by density and relative intensity measurements of the diffraction line having $d = 8.616$Å. A mechanism for the oxidation of bassetite is proposed. With increasing degree of oxidation, the solubility decreases markedly. From zeta-potential and surface conductivity measurements at 25°C, it is clear that the surfaces of mineral particles are negatively charged and not affected by oxidation. The point of zero charge for both synthetic bassetite and fully oxidized synthetic bassetite is reached at pH = 3.0 and 4.0 respectively. ^{57}Fe Mössbauer spectra are reported for synthetic bassetite and partially and fully oxidized synthetic bassetites, from which the oxidation degree may be determined.

Introduction

Bassetite belongs to the series of uranyl phosphates and has the crystal-chemical formula $Fe^{2+}[UO_2|PO_4]_2 \cdot nH_2O$ in which n varies from 8 to 12 for the meta and fully hydrated form respectively. This secondary uranyl phosphate is named after its type locality Wheal Basset, Redruth, Cornwall, England and was first described by Hallimond (1916), who found that bassetite from this locality frequently shows intergrowths with uranospathite and torbernite. Bassetite is also found in small quantities in the Fuemrol mines, Temple Mountain, Emery County, Utah (Roberts et al., 1974,) Denise mine, Green river, Emery County, Utah (Weeks and Thompson, 1954) and La Crouzille, Puy-de-Dôme, France (Branche et al., 1951). The mineral occurs often in the presence of pyrite and associated with uraninite.

According to Frondel (1954), bassetite belongs to the monoclinic system with cell parameters: $a = 6.98(4)$, $b =$

17.07(4), $c = 7.01(7)$Å, $\beta = 90°32' \pm 5'$ and unknown space group. Strunz (1977) classified the mineral in the uranite series with the tetragonal space group $I4/mmm$. Bassetite is not fluorescent, while uranospathite shows a green-yellow fluorescence under short and long ultra-violet radiation (Walenta, 1978). Due to the fact that bassetite sometimes shows intergrowths with uranospathite, some specimens however seem strongly fluorescent.

Data on specific gravity differ considerably: 3.10 g/cm^3 (Hallimond, 1916) and 3.40 g/cm^3 (Frondel, 1954).

Bassetite is rarely found in nature. This explains why studies on this mineral are rather scarce and why important properties, such as thermal behavior, stability against oxidation, Mössbauer spectra, etc., are unknown at the moment. This lack of knowledge supports the preparation of synthetic bassetite, and in this paper, the authors describe a new method of synthesis. Since bassetite can be oxidized very easily and no information about this feature is available, a substantial part of the present study deals with the oxidation process. Experimental methods, such as X-ray diffraction, ^{57}Fe Mössbauer- and infrared spectroscopy have been applied to study and characterize the synthetic bassetite and its oxidized phases. The solubility, double layer potential, and thermal stability have been determined as well.
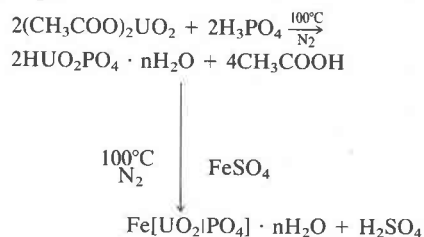
Synthesis

In this section, we discuss the synthesis of bassetite starting from pure chemicals and the transformation by ion exchange experiments on synthetic hydrogen autunite $H[UO_2|PO_4] \cdot 4H_2O$ and synthetic meta-autunite $Ca[UO_2|PO_4]_2 \cdot 7H_2O$ (Vochten and Deliens, 1980) into bassetite. All experiments involved were carried out in a nitrogen atmosphere and in the presence of ascorbic acid in order to avoid any oxidation.
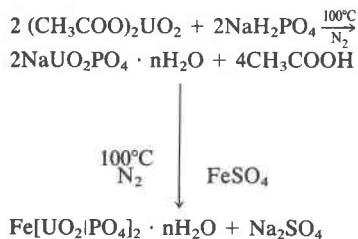
Synthesis from pure chemicals

To a boiling solution of 1 liter FeSO$_4 \cdot 7H_2O$ (0.075 mol/liter) containing 0.5% ascorbic acid, 1 liter $(CH_3COO)_2UO_2 \cdot 2H_2O$ (0.025 mol/liter) and 1 liter H_3PO_4 (0.03 mol/liter) are added simultaneously at a constant rate of 200 ml/hr. When this addition is completed, the reaction mixture is refluxed for 12 hours. The precipitate is filtered off, washed with distilled water and dried in a desiccator on silica gel in a constant stream of nitrogen. By chemical analysis and X-ray diffraction the resulting olive-green non-fluorescent powder was determined to be bassetite.

The formation of bassetite in this way can be described by the following reactions:

$$2(CH_3COO)_2UO_2 + 2H_3PO_4 \xrightarrow[N_2]{100°C}$$
$$2HUO_2PO_4 \cdot nH_2O + 4CH_3COOH$$

$$\downarrow \quad \begin{array}{c} 100°C \\ N_2 \end{array} \quad FeSO_4$$

$$Fe[UO_2|PO_4] \cdot nH_2O + H_2SO_4$$

Instead of H_3PO_4, $NaH_2PO_4 \cdot H_2O$ can also be used which leads to

$$2(CH_3COO)_2UO_2 + 2NaH_2PO_4 \xrightarrow[N_2]{100°C}$$
$$2NaUO_2PO_4 \cdot nH_2O + 4CH_3COOH$$

$$\downarrow \quad \begin{array}{c} 100°C \\ N_2 \end{array} \quad FeSO_4$$

$$Fe[UO_2|PO_4]_2 \cdot nH_2O + Na_2SO_4$$

It is clear that the formation of bassetite involves an intermediate formation of hydrogen autunite or sodium autunite.

Transformation of hydrogen autunite and meta-autunite into bassetite

If hydrogen autunite or meta-autunite is refluxed for 24 hours in a nitrogen atmosphere with a solution of FeSO$_4 \cdot 7H_2O$ 0.04 mol/liter containing 0.5% ascorbic acid both uranyl phosphates are completely transformed into bassetite. The transformation of meta-autunite can be represented as:

$$Ca[UO_2|PO_4]_2 \cdot nH_2O + FeSO_4 \xrightarrow[N_2]{100°C}$$
$$Fe[UO_2|PO_4]_2 \cdot nH_2O + CaSO_4$$
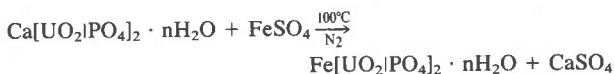
In order to avoid any contamination with CaSO$_4$, the product was filtered off and resuspended in a nitrogen atmosphere for 24 hours in a boiling solution of 0.5% EDTA, containing 0.5% ascorbic acid. From these experiments it is clear that the formation of bassetite can be explained as a primary formation of hydrogen autunite followed by an exchange reaction of the H$^+$ ions with Fe^{2+} ions.

Preparation of oxidized bassetite

Oxidized bassetite is easily prepared by the reaction of bassetite with a 0.6% H_2O_2 solution at room temperature, resulting in a yellow, non-fluorescent powder. The degree of oxidation can be varied continuously by varying the duration of the reaction.

X-ray crystallography

X-ray diffraction data have been obtained at 40 kV and 20 mA using a Philips PW 1140 generator and CuKα_1-radiation ($\lambda = 1.5406$Å). The photographs were recorded by means of a Guinier–Hägg camera with a diameter of 100 mm. Silicon powder (NBS-640) was used as an internal X-ray diffraction standard. The relative intensity of the diffraction lines was measured with a Carl Zeiss Jena MD-100 microdensitometer. From the calculated d_{hkl}-values the cell dimensions and cell volume were computed according to the method of McMasters and Larsen (1964). The powder patterns were indexed with the computer program of Visser (1969). Because of the very small size of the synthetic crystals of both bassetite

and its oxidized phases, neither single crystal diffraction data nor optical characteristics could be obtained.

Synthetic bassetite

Using the cell parameters given by Frondel (1954) $a = 6.98(4)$, $b = 17.07(4)$, $c = 7.01(7)$Å, $\beta = 90°32' \pm 5'$ as input to the indexing computer program of Visser (1969), 20 out of the 21 observed reflections could be indexed for which $\triangle Q_{obs.} \leq \triangle Q_{calc.}$ ($\triangle \theta \leq 0.05°$). The spacing data for synthetic bassetite are summarized in Table 1. Due to the fact that all 20 indexed lines meet the conditions $k = 2n$ for $0k0$ and hkl, we may conclude that synthetic bassetite belongs to the monoclinic system probably with space group $P2_1/m$ (C_{2h}^2). The density measured in toluene as 3.63 g/cm^3 is identical with the value calculated for a unit cell content of $Z = 2$ and a cell volume of 835.2Å.

Oxidized synthetic bassetite

The powder diffraction data obtained from fully oxidized synthetic bassetite are presented in Table 2. The cell parameters were calculated to be $a = 6.958(5)$, $b = 6.943(5)$, $c = 21.052(5)$Å, $\beta = 90°92' \pm 5'$, which indicates monoclinic symmetry. Taking these values in the indexing computer program of Visser (1969), all 22 reflections are indexed for which $\triangle Q_{obs.} \leq \triangle Q_{calc.}$ ($\triangle \theta \leq 0.05°$). Due to the fact that the extinction conditions corresponding to · different monoclinic space groups were observed to hold

Table 1. X-ray powder diffraction data for synthetic bassetite. Guinier-Hägg camera (diameter 100mm), CuKα_1-radiation (λ = 1.5406Å), 40 kV–20 mA.

I/I$_o$	d(obs.)	d(calc.)	h	k	l
100	8.616	8.535	0	2	0
70	4.9611	4.9691	$\bar{1}$	0	1
8	4.3106	4.2943	$\bar{1}$	2	1
76	3.4818	3.4898	$\bar{2}$	0	0
50	2.9479	2.9501	$\bar{1}$	2	2
		2.9433	$\bar{2}$	2	1
14	2.5363	2.5311	$\bar{1}$	4	2
46	2.4697	2.4689	$\bar{1}$	6	1
		2.4632	1	6	1
96	2.2162	2.2142	$\bar{3}$	0	1
38	1.7481	1.7511	$\bar{1}$	6	3
		1.7474	$\bar{3}$	6	1
		1.7450	1	6	3
28	1.6538	1.6563	$\bar{3}$	0	3
42	1.5665	1.5678	$\bar{4}$	0	2
22	1.5441	1.5459	$\bar{2}$	2	4
		1.5441	$\bar{3}$	4	3
		1.5420	$\bar{4}$	2	2
6	1.5272	———			
8	1.4723	1.4716	$\bar{4}$	4	2
52	1.3947	1.3959	$\bar{5}$	0	0
		1.3940	0	12	1
		1.3938	1	12	0
		1.3935	3	0	4
10	1.3837	1.3834	0	2	5
4	1.3737	1.3753	3	2	4
		1.3737	4	2	3
		1.3731	$\bar{4}$	6	2
		1.3720	1	0	5
4	1.3337	1.3339	$\bar{4}$	4	3
6	1.2381	1.2394	$\bar{1}$	6	5
		1.2372	5	4	2
2	1.2214	1.2202	4	10	0
2	1.1669	1.1667	3	8	4
		1.1657	4	8	3

Table 2. X-ray powder diffraction data for fully oxidized synthetic bassetite. Guinier–Hägg camera (diameter 100mm), CuKα_1-radiation (λ = 1.5406Å), 40 kV–20 mA.

I/I$_o$	d(obs.)	d(calc.)	h	k	l
85	10.359	10.525	0	0	2
23	5.8679	5.8472	$\bar{1}$	0	2
90	4.9422	4.9352	0	1	3
36	4.4578	4.4724	$\bar{1}$	1	2
23	3.5992	3.6123	$\bar{1}$	1	4
		3.5998	0	1	5
100	3.4843	3.4785	$\bar{2}$	0	0
		3.4715	0	2	0
57	3.3133	3.3188	$\bar{2}$	0	2
8	2.8503	2.8585	$\bar{2}$	1	3
		2.8479	$\bar{1}$	2	3
33	2.4629	2.4676	0	2	6
		2.4604	0	1	8
		2.4572	2	2	0
31	2.3937	2.3989	$\bar{2}$	2	2
77	2.2010	2.2062	1	0	9
		2.1996	3	1	0
		2.1979	0	3	3
		2.1960	1	3	0
51	2.1578	2.1597	$\bar{3}$	1	2
		2.1528	1	2	7
18	2.0244	2.0281	0	3	5
		2.0238	$\bar{1}$	0	10
		2.0235	$\bar{2}$	2	6
		2.0231	$\bar{2}$	1	8
		2.0230	1	3	4
2	1.8635	1.8658	$\bar{3}$	2	3
		1.8657	$\bar{1}$	3	6
		1.8623	$\bar{2}$	3	3
		1.8620	1	2	9
2	1.8533	1.8565	2	1	9
		1.8538	2	3	3
		1.8531	3	2	3
		1.8509	3	1	6
		1.8508	$\bar{3}$	0	7
3	1.7403	1.7393	4	0	0
		1.7378	0	3	8
5	1.7212	1.7205	$\bar{4}$	0	2
4	1.5584	1.5591	3	3	4
		1.5577	0	4	6
		1.5572	0	3	10
		1.5562	2	0	12
15	1.3654	1.3656	$\bar{3}$	4	3
		1.3643	3	1	0
		1.3642	1	4	9
8	1.2935	1.2946	3	1	13
		1.2945	1	5	5
		1.2942	2	0	15
		1.2926	0	1	16
10	1.2353	1.2359	$\bar{4}$	3	8
		1.2351	$\bar{2}$	5	5
		1.2351	5	1	7
		1.2342	2	3	13
2	1.2287	1.2296	5	2	5
		1.2286	4	4	0
		1.2281	0	5	8

for a limited number of diffraction lines, an exact determination of the space group turned out to be impossible. The density measured in toluene as 3.00 g/cm^3 agrees well with the value calculated for a unit cell content of $Z = 2$ and a cell volume of 1016.9Å^3.

After treatment of synthetic bassetite with 0.6% H_2O_2 for different time intervals, partially oxidized bassetites were obtained. Their degree of oxidation was determined from the ^{57}Fe Mössbauer spectra, which will be further discussed in the section on Mössbauer spectroscopy. With increasing degree of oxidation, both the density and the relative intensity of the diffraction line having $d = 8.616$Å decrease considerably but remain nearly constant
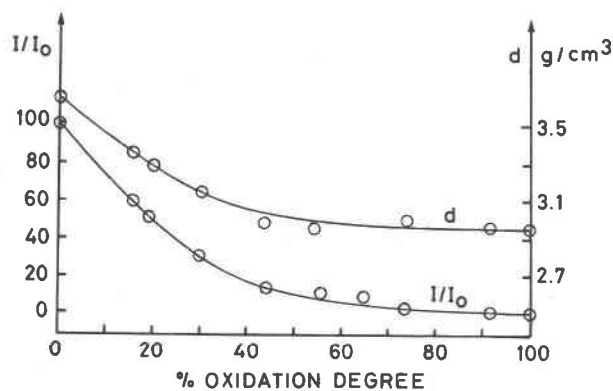
Fig. 1. Variation of relative intensity of the diffraction line having $d = 8.616$Å and density as a function of degree of oxidation of synthetic bassetite in 0.6% H_2O_2 medium.

for a degree of oxidation exceeding approximately 40%. These effects are illustrated for synthetic bassetite, treated with 0.6% H_2O_2, in Figure 1 and will be further discussed in the Section Mössbauer spectroscopy.

In conclusion, the cell parameters change significantly upon oxidation although the cell content remains the same. Furthermore, all investigated bassetite specimens belong to the monoclinic system.

Chemical composition

Methods

The air dried specimens of synthetic bassetite and its fully oxidized phase were dissolved in 6NHCl in nitrogen atmosphere. In this solution FeO, Fe_2O_3, UO_3 and P_2O_5 were determined. The H_2O content was determined on separate samples by thermogravimetric analysis.

The FeO content was determined according to the modified titrimetric method of Pratt (1894), whereby the ferrous iron is titrated in a boric-phosphoric acid medium with $K_2Cr_2O_7$, using barium diphenylamine sulphonate as an indicator. The Fe_2O_3 content is calculated from the difference between the ferrous and total iron, which is determined by the method of Hume and Kolthoff (1957).

The P_2O_5 content was determined by the spectrophotometric procedure of Michelsen (1957), based upon the yellow color induced by phosphorus with vanadomolybdate as reagent. The optical density was measured at 460 nm at which the interference from iron is strongly reduced or even eliminated completely. The UO_3 content was also determined spectrophotometrically with arsenazo III as reagent, the optical density being measured at 662.5 nm (Jeffery, 1975, p. 481–482).

Crystal-chemical formula

Table 3 summarizes the results of the analyses obtained as described above, together with the calculated oxide and crystal-chemical formula. From the total water content the hydration degree was calculated for synthetic bassetite and fully oxidized synthetic bassetite as 7 and 6 moles of water respectively. From the FeO, Fe_2O_3, UO_3, P_2O_5 and H_2O contents the corresponding oxide and crystal-chemical formulae were calculated by the residual oxygen method. According to Bulach (1964) this method is indeed most suited for the determination of formulae of minerals containing structural H_2O, OH^- or H_3O^+.

Mössbauer spectroscopy

Experimental

^{57}Fe Mössbauer spectra at room temperature and liquid nitrogen temperature were obtained on a time-mode spectrometer with constant acceleration drive and a triangular reference signal. ^{57}Co in a Rh matrix with an initial activity of 50 mCi was used as radiation source and was always kept at room temperature. The absorber compounds were finely ground, mixed with very pure carbon and spread out over the support in a uniform thickness of less than 5 mg Fe/cm^2. Spectra were run until a background of more than 10^6 counts per channel was reached. The total number of channels was 1024. The spectrometer was calibrated by simultaneously recording spectra of a standard metallic Fe foil, using a second ^{57}Co(Pd) source, mounted at the opposite side of the driving rod, and a separate counting system. The linearity of the spectrome-

Table 3. Chemical analyses of synthetic bassetite and its fully oxidized phase

| Oxide | Bassetite | | | Fully oxidized bassetite | | |
	Weight percent	Atomic quantities	Atomic ratio	Weight percent	Atomic quantities	Atomic ratio
FeO	8.01	0.1115	1.01	—	—	—
Fe_2O_3	—	—	—	9.01	0.1128	1.00
UO_3	63.69	0.2227	2.02	62.99	0.2202	1.94
P_2O_5	15.41	0.2171	1.97	15.04	0.2119	1.87
H_2O	13.84	—	7.01	13.46	—	6.50
Total	100.95			100.50		
Oxide formula	$FeO \cdot 2UO_3 \cdot P_2O_5 \cdot 7H_2O$			$Fe_2O_3 \cdot 2UO_3 \cdot P_2O_5 \cdot 6.5H_2O$		
Crystal-chemical formula	$Fe^{2+}[UO_2|PO_4]_2 \cdot 7H_2O$			$Fe^{3+}[UO_2|PO_4]_2(OH) \cdot 6H_2O$		

ter is better than 0.1% so that a linear least squares fitting for calibration purposes is more than sufficient. The velocity per channel was approximately 0.016 mm/sec. The linewidth of the innermost Fe-peaks was 0.25 to 0.27 mm/sec.

The Mössbauer parameters were determined by a least squares fitting of a sum of Lorentzian lines to the experimental Mössbauer spectra, using a modified version of the computer program of Chrisman and Tumolillo (1971). Absorption lines belonging to the same doublet were forced to have the same linewidth and intensity.

Results

Spectra at room temperature and liquid nitrogen temperature recorded on the non-oxidized synthetic bassetite sample are shown in Figure 2. The peculiar feature observed at low temperature, i.e., the appearance of a second Fe^{2+} doublet, was confirmed in a second run with a newly prepared absorber, and must therefore be ascribed to an intrinsic property of the material, indicating the presence of two distinct Fe^{2+} species.

Spectra at liquid nitrogen temperature for two partially oxidized bassetite samples are presented in Figure 3. They are a superposition of a sharp Fe^{2+} doublet (largest splitting) and a broad Fe^{3+} doublet (smallest splitting). The existence of two distinct Fe^{2+} doublets was not observed in the spectra of the partially oxidized samples
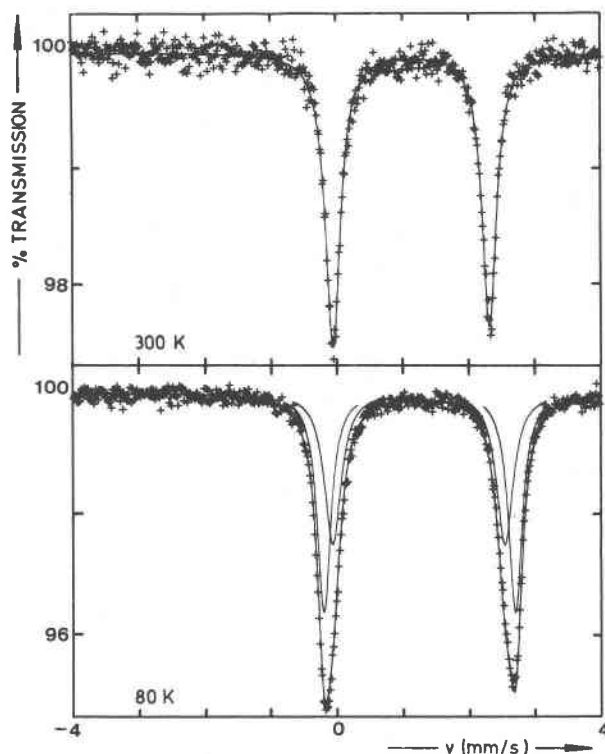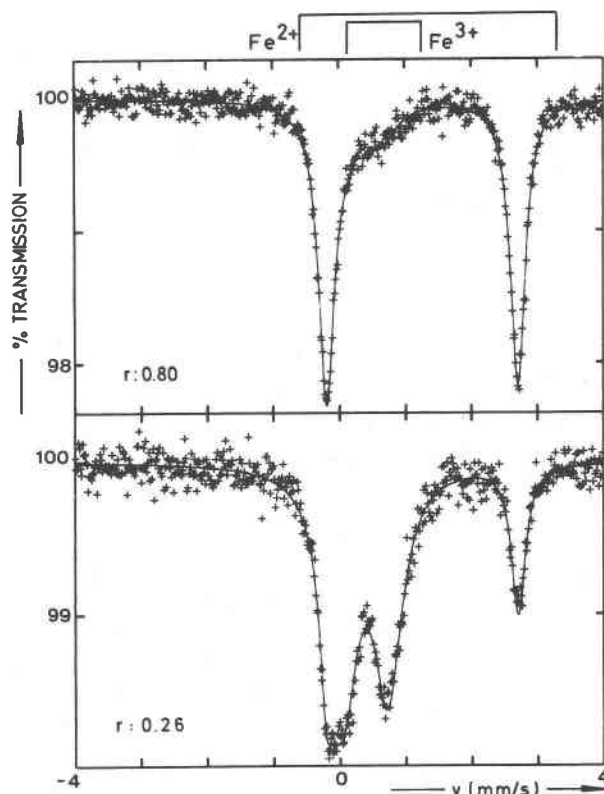

Fig. 3. Mössbauer spectra at $\simeq 80$ K for two partially oxidized synthetic bassetites. r is the Fe^{3+} content relative to the total Fe content.

although in some cases the larger Fe^{2+} linewidth (0.35 mm/sec) could indicate similar behavior. The fact that the oxidized samples originate from the same non-oxidized bassetite which definitely exhibits two Fe^{2+} species at low temperature, indicates a rather unusual behavior, the understanding of which will require much more systematic investigation, starting with a complete temperature dependent Mössbauer study. Moreover, because these features are irrelevant to the scope of the present Mössbauer measurements, i.e. the determination of the degree of oxidation and the relation between the latter and the average hyperfine parameters, it was decided not to include in the present work a detailed analysis of the two Fe^{2+} doublets and to make it the subject of future research which is now in progress.

The hyperfine parameters for non-oxidized synthetic bassetite are listed in Table 4. Table 5 contains the results for partially oxidized synthetic bassetite samples at $\simeq 80$ K classified according to increasing Fe^{3+} content. The identification number of each sample refers to the time during which the non-oxidized sample was in contact with the H_2O_2 solution (M = minutes, H = hours). As seen, there exists no unique relation between this duration and the final degree of oxidation.

The value of the degree of oxidation mentioned in the previous sections, was determined with the assumption

Fig. 2. Mössbauer spectra at $\simeq 80$ K and at $\simeq 300$ K for non-oxidized synthetic bassetite.

Table 4. Hyperfine parameters for non-oxidized synthetic bassetite at $\simeq 80$ K and at $\simeq 300$ K

T (K)	Doublet	ΔE_Q † mm/sec	δ ∷ mm/sec	Γ # mm/sec
$\simeq$ 300	Fe^{2+}	2.37(2)	1.20(1)	0.26(1)
$\simeq$ 80	Fe_I^{2+}	2.90(4)	1.32(2)	0.25(2)
	Fe_{II}^{2+}	2.61(4)	1.30(2)	0.31(2)

† $\Delta E_Q = 0.5\,e^2\,q\,Q$: quadrupole splitting
∷ δ : isomeric shift versus metallic Fe
Γ : line width
The errors equal three times the computed standard deviations

that the Fe^{3+}/Fe^{2+} atomic ratio equals the ratio between the relative areas of the corresponding doublets. It is well known that this procedure is only justified if the Mössbauer fractions for both Fe species are equal. This is only approximately true, even for Fe species within the same lattice and deviations as large as 10% can occur, especially at higher temperatures (300 K). At 80 K, the possible errors are much smaller. Further, the remaining deviations become less relevant on a relative base, i.e. when results obtained for a series of samples with similar structures are mutually compared.

Discussion

In view of the discussion regarding the Mössbauer results, it is necessary for the reader to have more insight into the peculiar bassetite structure.

Bassetite belongs to the metatorbernite subgroup of the layered structured uranium minerals (Povarennykh, 1972). The structure is built up in sheets consisting of PO_4 tetrahedrons and UO_6 octahedrons linked to each other by a common oxygen ion. The layers are held together mainly via hydroxyl–hydrogen bonds to H_2O molecules. The latter form squares between the layers at two different levels. Half of these squares surround a central Fe ion which is further linked to two O^{2-} ions in uranyl groups. The additional water molecules are distributed statistical-

ly between the sheets and largely determine the value of the c lattice parameter. A schematic representation of the assumed bassetite structure, if analogous to meta-autunite as described by Beintema (1938), is shown in Figure 4.

Both the Fe^{2+} quadrupole splitting ΔE_Q and the Fe^{2+} isomeric shift δ are consistent with octahedral coordination (Bancroft, 1973). The large value of ΔE_Q indicates an electronic singlet ground state which further indicates a trigonally or tetragonally compressed octahedron (Dockum and Reiff, 1979). The rather small line widths for synthetic bassetite demonstrate that the distribution on the type and on the amount of compression is quite narrow.

As pointed out above, the presence of two distinct Fe^{2+} doublets, probably arising from two different Fe^{2+} species, is not yet understood and any suggestion regarding a possible mechanism causing this peculiar feature, remains highly speculative at the moment.

The Fe^{2+} hyperfine parameters for partially oxidized synthetic bassetites at $\simeq 80$ K are very similar to those of the Fe_I^{2+} doublet for the non-oxidized sample. So, whereas the oxidation prevents the occurence of a second Fe^{2+} species, it does not alter the average symmetry of the local surrounding. Some line broadening, though, is observed for a few samples, in particular for 30 H and, to a lesser extent, for 10 H. It is not believed that this is due to the presence of a second but unresolved Fe^{2+} doublet, as observed in the case of non-oxidized synthetic bassetite, because if this were true, the quadrupole splitting would indeed be more shifted towards the lower value (i.e., 2.61 ± 0.04 mm/sec) of the Fe_{II}^{2+} quadrupole splitting. Therefore, it is suggested that the oxidation process causes a broader range of possible distortions for the Fe^{2+} coordinations, however without shifting the average value of it as both ΔE_Q and δ are clearly not affected by the Fe^{3+} concentration.

The Fe^{3+} hyperfine parameters are also typical for an octahedral $(H_2O)_4O_2$ coordination (Vochten et al., 1979). The linewidths however are much larger than in the case of Fe^{2+} and indicate a broad range of possible distortions

Table 5. Mössbauer parameters for partially oxidized synthetic bassetite samples at $\simeq 80$ K

Sample	Fe^{2+}				Fe^{3+}			
	ΔE_Q † mm/sec	δ ∷ mm/sec	Γ # mm/sec	RA ∅	ΔE_Q † mm/sec	δ ∷ mm/sec	Γ # mm/sec	RA ∅
30 M	2.89(1)	1.31(1)	0.25(1)	0.84(3)	0.8 (1)	0.41(1)	0.8 (3)	0.16(3)
20 H	2.90(2)	1.32(1)	0.28(1)	0.80(3)	0.6 (1)	0.41(7)	0.6 (1)	0.20(3)
55 H	2.83(6)	1.31(3)	0.34(2)	0.78(3)	0.67(8)	0.45(4)	0.5 (1)	0.22(3)
6 H	2.90(3)	1.32(1)	0.32(3)	0.56(4)	0.64(7)	0.43(3)	0.53(7)	0.44(4)
10 H	2.87(3)	1.32(1)	0.35(3)	0.44(3)	0.70(4)	0.45(2)	0.60(5)	0.56(3)
30 H	2.84(3)	1.33(2)	0.45(5)	0.35(2)	0.67(3)	0.46(2)	0.66(4)	0.65(2)
25 H	2.91(3)	1.32(2)	0.26(3)	0.26(3)	0.68(3)	0.45(2)	0.52(3)	0.74(3)
40 H	2.8 (1)	1.26(6)	0.3 (1)	0.08(3)	0.78(3)	0.47(2)	0.59(4)	0.92(3)

† $\Delta E_Q = 0.5\,e^2\,q\,Q$: quadrupole splitting
∷ δ : isomeric shift versus metallic Fe
Γ : line width
∅ RA: relative area
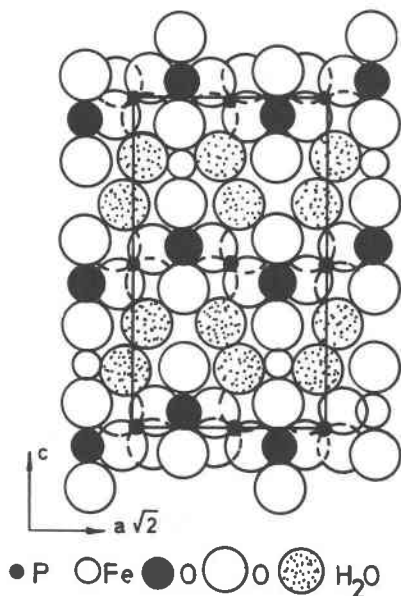The errors equal three times the computed standard deviations

Fig. 4. Assumed structure of bassetite after metaautunite.

of the Fe^{3+} coordinations, probably caused by the non-uniform location of the hydroxyl group which replaces H_2O when Fe^{2+} is oxidized to Fe^{3+}.

The significant difference between the Fe^{2+} and Fe^{3+} linewidths suggests that the oxidation is not uniform. It is believed that complete oxidation takes place at the outer surface layers first whereas the bulk of the grains remains unaltered. The oxidation then proceeds progressively towards the inner part of the grains with increasing duration of exposure to the H_2O_2 solution. The oxidation kinetics for such a mechanism probably depend upon a great many factors, such as surface condition, grain size, etc., and the degree of oxidation is therefore not simply related to the exposure time.

The proposed oxidation mechanism very well accounts for the observed behavior of the density and the d_{hkl}-value $= 8.616\text{Å}$ as a function of the measured average oxidation degree. It may also explain the increasing line width of the Fe^{2+} doublet arising from the non-oxidized part of the particles. Indeed, because the crystal structure of completely oxidized bassetite differs significantly from the one of non-oxidized bassetite, non-uniform internal stresses in the non-oxidized bulk part of the grains are induced by the oxidation of the outer part of the grains, leading to fluctuations in the local environment of the Fe^{2+} ions and broadening of the Mössbauer absorption lines. These effects become more pronounced when the contribution of the completely oxidized part increases at the expense of the non-oxidized bulk part.

Infrared spectroscopy

The infrared spectra of both minerals in KBr pellets were recorded by means of a Beckman infrared spectrophotometer type 4240 covering the range from 4000 to 400 cm^{-1}.

The spectrum of synthetic bassetite and fully oxidized synthetic bassetite are shown in Figure 5A and Figure 5B respectively. The infrared spectra of both minerals are quite simple and very similar. However small, but significant differences are observed in the regions 3600 to 2700 cm^{-1} and 1650 to 1600 cm^{-1} and will be discussed below.

The vibration modes of the tetrahedral PO_4-group are well known: ν_1: PO-stretching (940 cm^{-1}), ν_2: OPO-bending (420 cm^{-1}), ν_3: PO-stretching (1020 cm^{-1}), ν_4: OPO-bending (560 cm^{-1}) (Gonzalez-Diaz and Santas, 1978). Normally only the ν_3 and ν_4 vibrations are infrared active. However, the inactive modes may become active by distortion of the tetrahedral symmetry of the PO_4-groups. As can be seen from Figures 5A and 5B, the frequencies attributed to the PO_4-group are the same for both minerals. The lack of significant changes in these
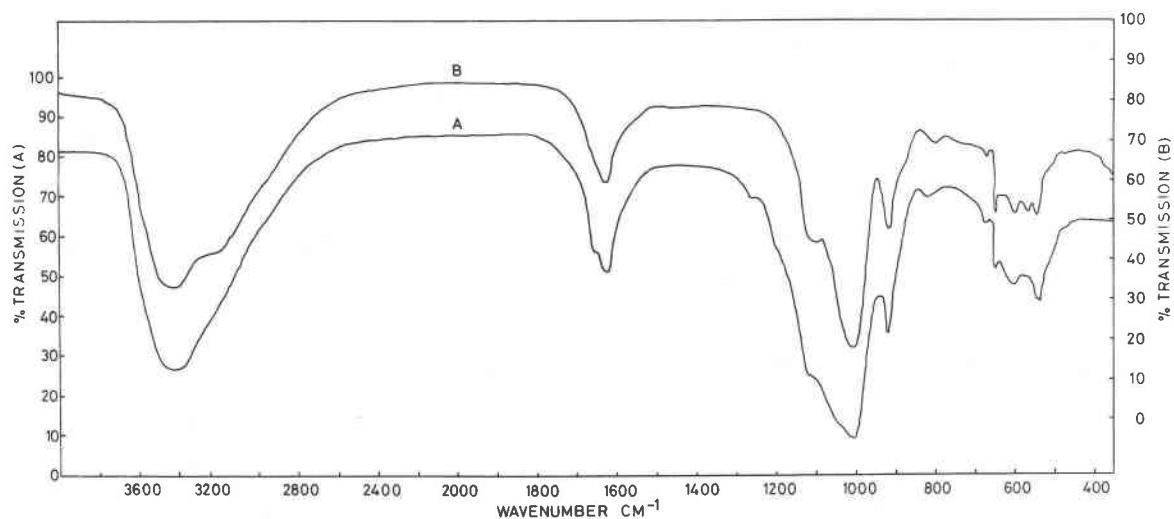

Fig. 5. Infrared spectrum of synthetic bassetite (A) and fully oxidized synthetic bassetite (B).
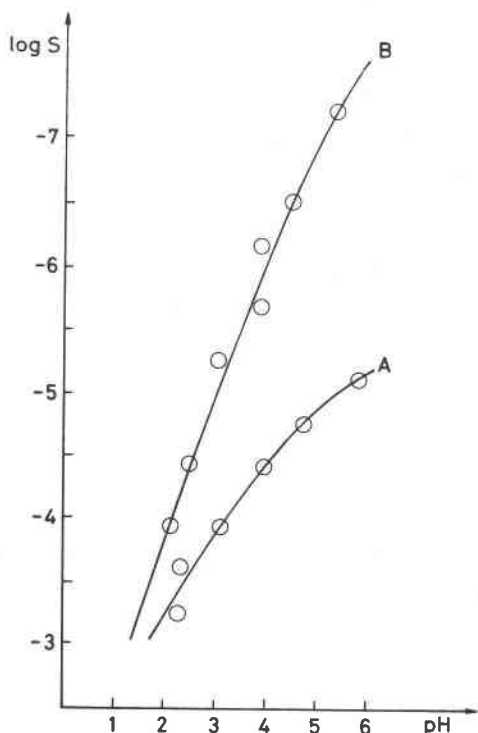
Fig. 6. Variation of logarithm of solubility at 25°C for synthetic bassetite (A) and fully oxidized synthetic bassetite (B) as a function of the pH.

bands would indicate that, to a large extent the PO_4^{3-} local symmetry remains unchanged upon oxidation.

As known (see also section Thermal behavior), there are several non-equivalent H_2O molecules present in the structure, resulting in distinct intermolecular hydrogen bonds. Indeed, a correlation exists between the O—H---O length and the $\nu(OH)$; decreasing O---O distances result in decreasing OH stretching frequencies (Lippincott et al., 1959). Water molecules give bands in the regions 1600–1650 cm^{-1} ($\nu_2(H_2O)$ bending vibration) and 2600–3700 cm^{-1} ($\nu_1(H_2O)$ and $\nu_3(H_2O)$ stretching vibration). For both compounds, the shape of the band in the H_2O bending region is nearly the same. Only one band is observed for fully oxidized synthetic bassetite, while a small shoulder on that band is present for synthetic bassetite. On the contrary, the shape of the high frequency band is different for the two mineral specimens: one broad band is observed for synthetic bassetite, while for its fully oxidized state a shoulder appears in the low frequency part of that band. The broad high frequency OH band is produced by contributions of both coordinated and lattice water. The difference between the OH band of each compounds is related to changes occuring in the coordinated water molecules. From the relation $Fe(H_2O)^{2+} \rightarrow Fe^{3+}OH^-$, it follows that two factors must be considered: an increase of the electronic charge on the cation and the presence of an OH^- group instead of a

H_2O molecule. The influence of the charge of the cation on the OH-frequency is thoroughly discussed by various authors (Brink, 1972; Maltese and Orville-Thomas, 1967). An increase in the charge of the cation results in a shift of the electronic charge of the oxygen atom in the OH^- group of water towards the metal atom. As a consequence, lower frequencies are observed for these OH^- groups. This can explain the appearance of the shoulder in the low frequency part of the OH band. Further, we have to consider the change of a H_2O molecule into a OH^- group. The frequency characteristic for OH^- groups lies in the region 3500–3600 cm^{-1}. No change in the band between the two compounds is found in that region. So we conclude that the difference in the OH band shape is almost entirely due to the difference in electronic charge of the cation between the two compounds.

Solubility and electrokinetic properties

Solubility

In order to explain the observed variation of the zeta-potential as a function of the pH, discussed in the next subsection, the solubility of synthetic bassetite and fully oxidized synthetic bassetite was studied as a function of the pH, in the range 2.4 to 6. For that purpose, the aqueous suspensions in HCl-medium were equilibrated at 25°C in a nitrogen atmosphere for one week. After filtration of the suspensions, the pH of the filtrate was measured and the iron content was determined by atomic absorption spectrometry.

In Figure 6 the variation of the solubility at 25°C is plotted versus the pH. It shows that the solubility for fully oxidized synthetic bassetite is much lower than for non-oxidized synthetic bassetite. For both minerals, the solubility increases markedly in acid medium.

Electrokinetic properties

In order to obtain information about the surface structure of the mineral particles in suspension, the zeta-potential was measured at 25°C at different pH-values.

Theory. Theoretical considerations concerning the zeta-potential and the surface conductivity are discussed by Vochten et al. (1979).

In suspension, the mineral particles build up an electrical double layer for which the zeta-potential can be calculated as:

$$\zeta = \frac{112890}{D} \eta u \qquad (1)$$

where D is the relative dielectric constant of the solvent, η the viscosity of the solvent in poise, u the electro-osmotic mobility of the solvent with respect to the surface of the particle in $\mu m \cdot sec^{-1}/V \cdot cm^{-1}$ and ζ the zeta-potential in mV.

The surface conductivity λ_s in Ω^{-1} may be written as:

$$\lambda_s = \sqrt{\frac{DRTC}{2\pi F^2}} \left[(e^{\frac{F}{2RT}\zeta} - 1) \left(v_c F + \frac{DRT}{2\pi\eta} \right) \right.$$

$$\left. + (e^{\frac{F}{2RT}\zeta} - 1) \left(v_a F + \frac{DRT}{2\pi\eta} \right) \right] \quad (2)$$

the determination of which requires an accurate knowledge of the zeta-potential. In expression (2) the different symbols are defined as follows:

> D: relative dielectric constant of the solvent;
> R: gas constant;
> T: temperature in K;
> C: concentration of the ions in the bulk phase in mol/cm^3;
> F: Faraday constant;
> $v_c F$ and $v_a F$: specific conductivity of the cations and anions involved, in cm^2/mol.

The term $(DRT)/(2\pi\eta)$ represents the electro-osmotic motion of the solvent on the two kinds of ions.

Experimental. The micro-electrophoretic mobilities of the particles in suspension were measured in a thermostated ($\pm 0.1°C$) cylindrical microelectrophoresis cell (Rank Brothers, Mark II) with microscopic magnification of 200. Platinum electrodes were used as measuring electrodes for which the polarity was reversed for each measurement. In order to remove any traces of organic material, the specimens were first washed with chloroform.

Since bassetite oxidizes very easily, the electrophoretic measurements were carried out in preboiled water in a nitrogen atmosphere. This procedure prevents any oxida-
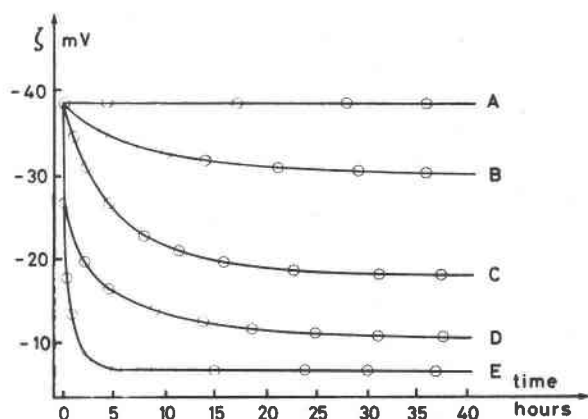
Fig. 7. Variation of zeta-potential as a function of time at 25°C for an aqueous suspension of synthetic bassetite. (A) nitrogen atmosphere, preboiled water, pH = 5.6; (B) air atmosphere; (C) nitrogen atmosphere, 0.03% H_2O_2; (D) nitrogen atmosphere, 0.06% H_2O_2; (E) nitrogen atmosphere, 0.10% H_2O_2.
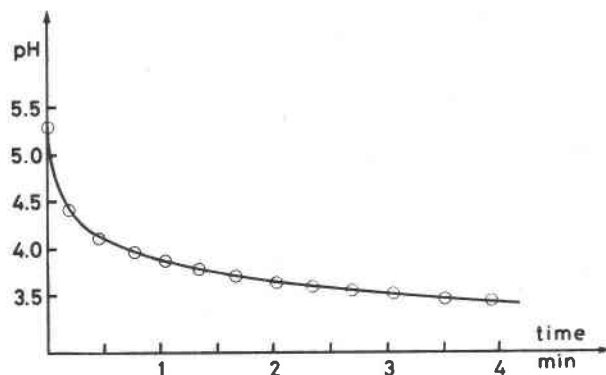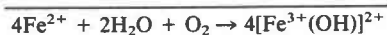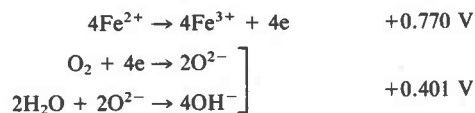
Fig. 8. Variation of pH at 25°C as a function of time for an aqueous suspension of fully oxidized synthetic bassetite (0.002 mol/liter).

tion and thus results in a time independent zeta-potential (Fig. 7A). If instead, the experiments are performed in water which is in equilibrium with the partial oxygen pressure of the air, the zeta-potential strongly depends on the time (Fig. 7B). The observed decrease of the zeta-potential as a function of time in the latter case can be explained by the partial oxidation of bassetite. As a consequence of this oxidation, the release of Fe^{3+} ions causes a strong hydrolytic effect, resulting in a decrease of the pH. This effect is nicely illustrated if fully oxidized synthetic bassetite (0.002 mol/liter) is suspended in water and the decrease of the pH is recorded as a function of time (Fig. 8).

In view of the present results the mechanism of the oxidation can be represented by the following electrochemical reactions

$$4Fe^{2+} \rightarrow 4Fe^{3+} + 4e \qquad +0.770 \text{ V}$$

$$\left. \begin{array}{l} O_2 + 4e \rightarrow 2O^{2-} \\ 2H_2O + 2O^{2-} \rightarrow 4OH^- \end{array} \right] \qquad +0.401 \text{ V}$$

$$\overline{4Fe^{2+} + 2H_2O + O_2 \rightarrow 4[Fe^{3+}(OH)]^{2+}}$$

Considering this mechanism, the partial oxidation of bassetite can be written as

$$4Fe^{2+}[UO_2|PO_4]_2 \cdot 7H_2O + xO_2 \rightarrow$$

$$4Fe^{2+}_{1-x}Fe^{3+}_x[UO_2|PO_4]_2(OH)_x \cdot (7-x)H_2O$$
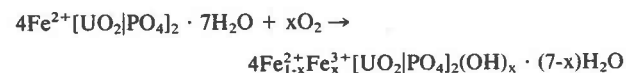
If x = 1, complete oxidation is established.

The oxidation of bassetite in an aqueous suspension can be accelerated by the presence of H_2O_2 which decomposes catalytically into H_2O and O_2. The effect of the H_2O_2 concentration on the oxidation rate of synthetic bassetite is indeed very clear in Figure 7: curves C, D and E for H_2O_2 concentrations of 0.03, 0.06 and 0.10% respectively. As a consequence of the oxidation and the subsequent hydrolysis of the Fe^{3+} ion, the pH of the suspension decreases markedly. The time dependence of the pH for a suspension of synthetic bassetite in different
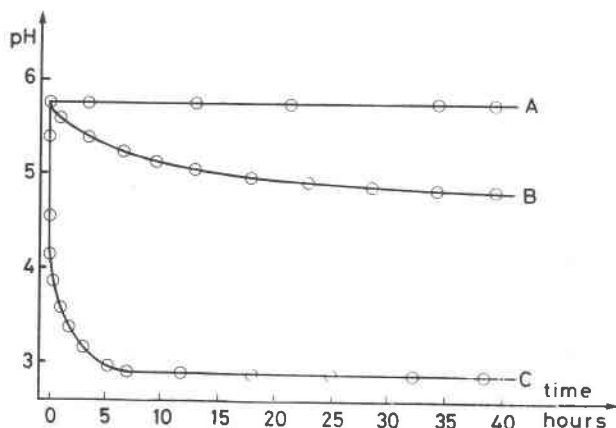
Fig. 9. Variation of pH at 25°C as a function of time for an aqueous suspension of synthetic bassetite (0.002 mol/liter) under different experimental conditions. (A) nitrogen atmosphere, preboiled water; (B) air atmosphere, distilled water; (C) nitrogen atmosphere, 0.10% H_2O_2.

experimental conditions is shown in Figure 9. It is well known that Fe^{2+} and Fe^{3+} ions undergo appreciable hydrolysis, with a marked effect on the solubility of their precipitates. Hedström (1952) deduced that hydrolysis of Fe^{2+} ions could be represented by the single reaction

$$Fe^{2+} + H_2O \rightleftharpoons [Fe(OH)]^+ + H^+ \quad (K = 3.10^{-10})$$

whereas that of the Fe^{3+} ions involves the following

reactions (Hedström, 1953)

$$Fe^{3+} + H_2O \rightleftharpoons [Fe(OH)]^{2+} + H^+ \quad (K_1 = 9.10^{-4})$$

$$[Fe(OH)]^{2+} + H_2O \rightleftharpoons [Fe(OH)_2]^+ + H^+ \quad (K_2 = 5.10^{-7})$$

$$2Fe^{3+} + 2H_2O \rightleftharpoons [Fe_2(OH)_2]^{4+} + 2H^+ \quad (K_3 = 1.10^{-3})$$

The equilibrium constants of the last three reactions are such that the dimeric species $[Fe_2(OH)_2]^{4+}$ is the major form of Fe^{3+}. From the different equilibrium constants it is clear that hydrolysis of the Fe^{2+} ion can be neglected in comparison with those of the Fe^{3+} ion.

From the experimental results regarding the zeta-potential and its relation with the pH, we may conclude that bassetite oxidizes very easily in an aqueous medium, even in the absence of strong oxidants. The effect of the pH on the zeta-potential both for synthetic bassetite and its fully oxidized phase is illustrated in Figure 10, for which the observations can be explained as follows: the H^+ ions formed by hydrolysis lead to a protonization of the negatively charged $(UO_2PO_4)_n^{n-}$-layers, resulting in a more positive zeta-potential. From the graphs of Figure 10 it is therefore clear that the oxidized phase of bassetite shows a stronger protonization as compared to non-oxidized bassetite. Contrary to behavior of other uranyl phosphates (Vochten et al., 1979, 1981; Vochten and
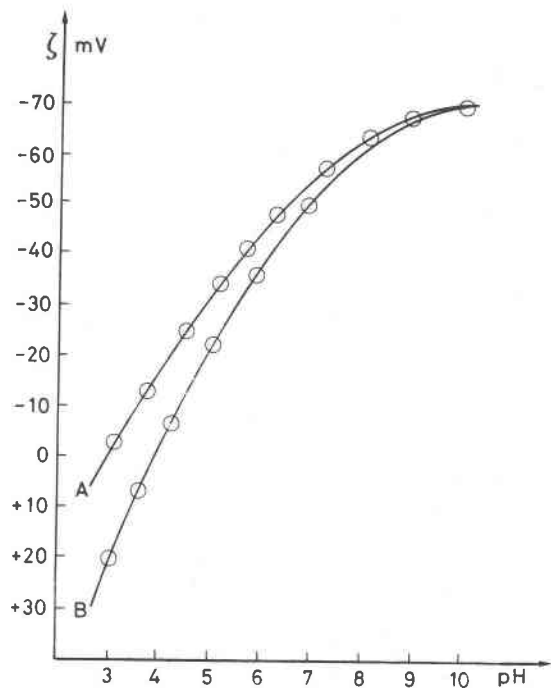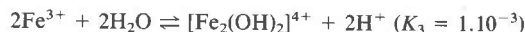

Fig. 10. Variation of the zeta-potential at 25°C as a function of pH for an aqueous suspension of synthetic bassetite (A) and fully oxidized synthetic bassetite (B).
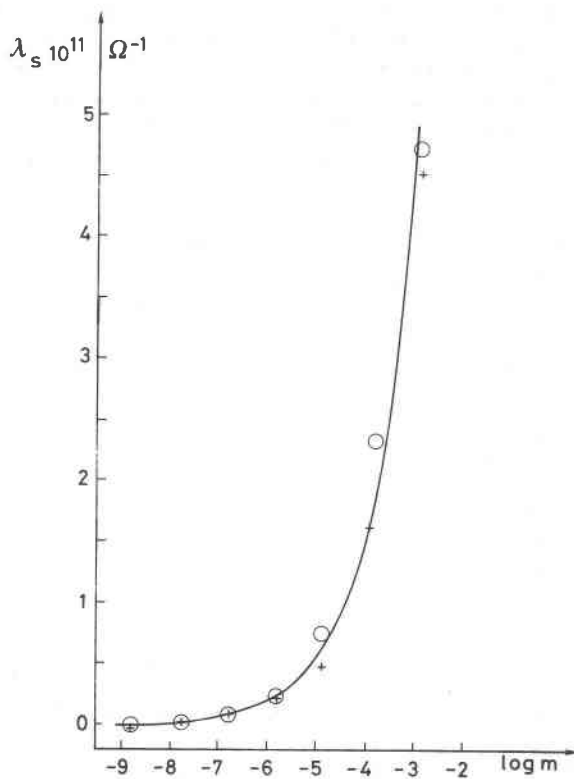

Fig. 11. Variation of the surface conductivity at 25°C and at pH = 5.2 for synthetic bassetite and fully oxidized synthetic bassetite as a function of the KCl concentration. m is expressed in mol/kg.

Deliens, 1980; Vochten and Pelsmaekers, 1983), the point of zero charge can be reached for synthetic bassetite and fully oxidized synthetic bassetite, more precisely at pH = 3.0 and 4.0 respectively (Fig. 10).

The surface conductivity at 25°C and at pH = 5.2, calculated from zeta-potential measurements in KCl-medium, shows no significant differences between synthetic bassetite and fully oxidized synthetic bassetite. The variation of the surface conductivity with KCl concentration is presented in Figure 11. Because the surface conductivity is the same for the two synthetic compounds, we may conclude that the surface structure of bassetite remains unaltered upon oxidation.

Thermal behavior

Since no data on the thermal behavior of bassetite and its fully oxidized phase are available from previous work, the thermal stability of both synthetic minerals was investigated by differential scanning calorimetric (DSC) and thermogravimetric analyses (TGA). These analyses were performed by means of a DuPont DSC-910 and TGA-951 apparatus in atmospheric conditions with a rate of heating of 10°C/min.

The DSC curves for synthetic bassetite and fully oxidized synthetic bassetite are presented in Figure 12A and Figure 12B respectively. They clearly display two distinct regions: an endothermic one and an exothermic one. The exothermic region, ranging from 250 to 400°C, corre-
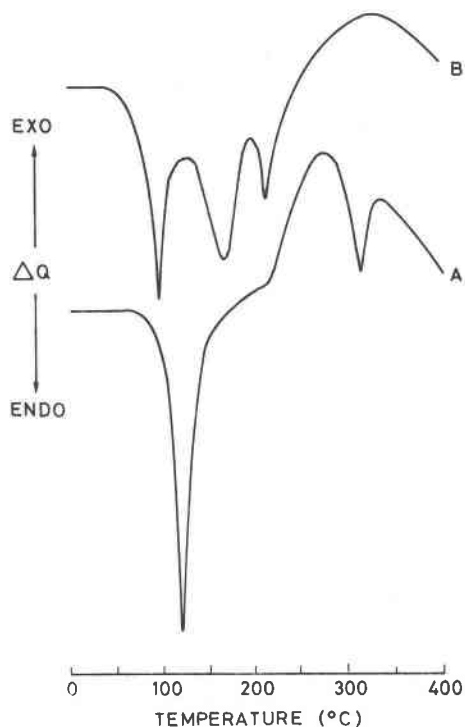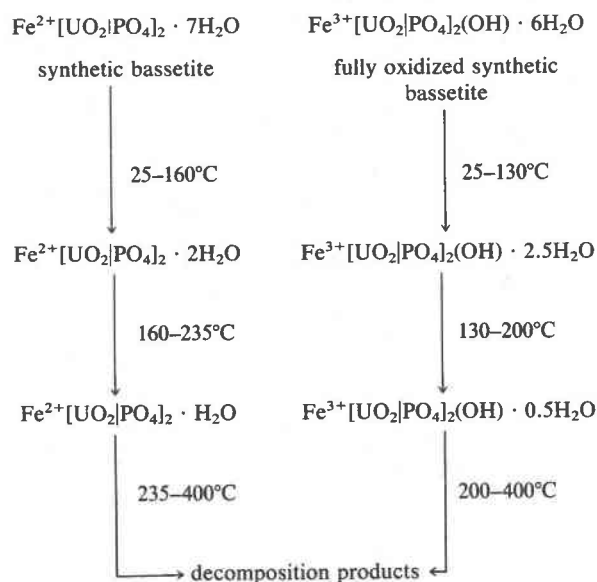
sponds to the exothermic formation of α-Fe_2O_3. The lower endothermic region reflects the different dehydration stages of the minerals. For synthetic bassetite, one of the endothermic dehydration peaks even occurs in the exothermic region, i.e., at 295°C, corresponding to a loss of one mole of water. The dehydration of fully oxidized synthetic bassetite was studied by DSC and TGA measurements combined with infrared spectroscopy at different temperatures, from which it is clear that the OH-group is released above 215°C.

The dehydration of the minerals can be represented by the following scheme:

$Fe^{2+}[UO_2|PO_4]_2 \cdot 7H_2O$ $Fe^{3+}[UO_2|PO_4]_2(OH) \cdot 6H_2O$

synthetic bassetite   fully oxidized synthetic bassetite

$\downarrow$ 25–160°C $\downarrow$ 25–130°C

$Fe^{2+}[UO_2|PO_4]_2 \cdot 2H_2O$ $Fe^{3+}[UO_2|PO_4]_2(OH) \cdot 2.5H_2O$

$\downarrow$ 160–235°C $\downarrow$ 130–200°C

$Fe^{2+}[UO_2|PO_4]_2 \cdot H_2O$ $Fe^{3+}[UO_2|PO_4]_2(OH) \cdot 0.5H_2O$

$\downarrow$ 235–400°C $\downarrow$ 200–400°C

$\longrightarrow$ decomposition products $\longleftarrow$

The number of H_2O molecules, lost in the different steps indicated, was determined from the corresponding TGA curves.

In conclusion, both bassetite and fully oxidized bassetite easily loose part of their water. The same conclusion was arrived at by Beintema (1938) in his study on autunite and meta-autunite specimens. It was also observed by this author that the transformation is quite reversible in the low temperature region.

Fig. 12. DSC curves for synthetic bassetite (A) and fully oxidized synthetic bassetite (B).

References

Bancroft, G. M. (1973) Mössbauer Spectroscopy: An Introduction for Inorganic Chemists and Geochemists. McGraw-Hill Company (UK) Ltd., London.

Beintema, J. (1938) On the composition and the crystallography of autunite and the meta-autunites. Receuil des Travaux Chimiques des Pays-Bas, 57, 155–175.

Branche, G., Chervet, J., and Guillemin, C. (1951) Nouvelles

espèces uranifères françaises. Bulletin de la Société Française de Minéralogie et de Cristallographie, 74, 457–488.

Brink, George (1972) Infrared studies of water in crystalline hydrates: $BaCl_2 \cdot 2H_2O$. Spectrochimica Acta, 28A, 1151–1155.

Bulach, A. G. (1964) Berechnung von Mineralformeln. VEB Deutscher Verlag für Grundstoffindustrie, Leipzig.

Chrisman, B. and Tumolillo, T. (1971) Computer Analysis of Mössbauer Spectra. Computer Physics Communications, 2, 322–330.

Dockum, B. W., and Reiff, W. M. (1979) A high field Mössbauer study of a six co-ordinate iron II dithiocarbamate complex and comparison of the $Fe(II)S_6$, $Fe(III)S_6$ and $Fe(IV)S_6$ chromophores in tris(diethyldithiocarbamate) complexation. Chemical Physics Letters, 63, 32–36.

Frondel, Clifford (1954) Bassetite and uranospathite. Mineralogical Magazine, 30, 343–353.

Gonzalez-Diaz, P. F. and Santas, M. (1978) Infrared spectra of strontium, lead and barium apatites. Spectrochimica Acta, 34A, 241–246.

Hallimond, A. F. (1916) On bassetite and uranospathite, new species hitherto classed as autunite. Mineralogical Magazine, 17, 221–236.

Hedström, B. O. A. (1952) The hydrolysis of the iron(II) ion. Arkiv för Kemi, 5, 457–468.

Hedström, B. O. A. (1953) The hydrolysis of the iron(III) ion. Arkiv för Kemi, 6, 1–16.

Hume, David N. and Kolthoff, I. M. (1957) The use of cacotheline as an oxidation–reduction indicator before the volumetric oxidation of iron. Analytica Chimica Acta, 16, 415–418.

Jeffery, P. G. (1975) Chemical Methods of Rock Analysis. Pergamon Press, Oxford.

Lippincott, E. R., Finsch, J. N., and Schroeder, R. (1959) Hydrogen Bonding. Pergamon Press, Oxford.

Maltese, M., and Orville-Thomas, W. J. (1967) The infrared spectra and structure of some complex hydroxosalts. Journal of inorganic nuclear Chemistry, 29, 2533–2544.

McMasters, O. D. and Larsen, W. L. (1964) Determination of the crystallographic lattice type and cell constants from X-ray powder pattern data, a computer program. U.S. Atomic Energy Commission, Report IS-839.

Michelsen, Odd B. (1957) Photometric determination of phos-phorus as molybdovanadophosphoric acid. Analytical Chemistry, 29, 60–62.

Povarennykh, A. S. (1972) Crystal-chemical Classification of Minerals. Plenum Press, New York.

Pratt, J. H. (1894) On the determination of ferrous iron in silicates. American Journal of Science, XLVIII, Nr. 284, 149–151.

Roberts, W., Rapp, G., and Weber, J. (1974) Encyclopedia of Minerals. Van Nostrand Reinhold, New York.

Strunz, H. (1977) Mineralogische Tabellen. Akademische Verlagsgesellschaft, Geest und Portig K.-G., Leipzig.

Visser, J. W. (1969) Fully automatic program for finding the unit cell from powder data. Journal of Applied Crystallography, 2, 89–95.

Vochten, Renaud, De Grave, Eddy, and Stoops, Georges (1979) Petrographic, chemical and Mössbauer study of some oxidized vivianite nodules from Retie (Province of Antwerp, Belgium). Neues Jahrbuch für Mineralogie Abhandlungen, 137, 208–222.

Vochten, Renaud, and Deliens, Michel (1980) Transformation of curite into meta-autunite: paragenesis and electrokinetic properties. Physics and Chemistry of Minerals, 6, 129–143.

Vochten, Renaud, Huybrechts, Willy, and Remaut, Germain (1979) Formation of meta-torbernite starting from curite: crystallographic data and electrokinetic properties. Physics and Chemistry of Minerals, 4, 281–290.

Vochten, Renaud and Pelsmaekers, Jozef (1983) Synthesis, solubility, electrokinetic properties and refined crystallographic data of sabugalite. Physics and Chemistry of Minerals, 9, 23–29.

Vochten, Renaud, Piret, Paul, and Goeminne, Andre (1981) Synthesis, crystallographic data, solubility and electrokinetic properties of copper, nickel- and cobalt uranyl phosphate. Bulletin de Minéralogie, 104, 457–467.

Walenta, Kurt (1978) Uranospathite and arsenuranospathite. Mineralogical Magazine, 42, 117–128.

Weeks, A. D. and Thompson, M. E. (1954) Identification and occurence of uranium and vanadium minerals from the Colorado plateaus. U. S. Geological Survey, Bulletin 1009-B, 13–62.